frontiers | Frontiers in Materials

TYPE Original Research
PUBLISHED 15 December 2023
DOI 10.3389/fmats.2023.1318366

OPEN ACCESS

EDITED BY
Anbang Li,
Xi'an University of Architecture and Technology, China

REVIEWED BY
Kun Xu,
Beijing University of Technology, China
Yefei Ren,
China Earthquake Administration, China

*CORRESPONDENCE
Lang Liu,
janice_liu@cqjtu.edu.cn

RECEIVED 11 October 2023
ACCEPTED 27 November 2023
PUBLISHED 15 December 2023

CITATION
Wang X, Zhang G, Liu L, Li Y, Kong H and Zhang C (2023), Mechanical and fatigue properties of graphene oxide concrete subjected to sulfate corrosion.
Front. Mater. 10:1318366.
doi: 10.3389/fmats.2023.1318366

Mechanical and fatigue properties of graphene oxide concrete subjected to sulfate corrosion

Xu Wang[1,2], Guoliang Zhang[1,2], Lang Liu[1,2]*, Yongguang Li[1,2], Hu Kong[3] and Cheng Zhang[4]

[1]State Key Laboratory of Mountain Bridge and Tunnel Engineering, Chongqing Jiaotong University, Chongqing, China, [2]School of Civil Engineering, Chongqing Jiaotong University, Chongqing, China, [3]Department of Civil and Transportation Engineering, Hohai University, Nanjing, China, [4]Shenzhen Y. S. Mao Bridge Design Group Co Ltd., Shenzhen, China

Concrete structures usually have to experience some unfavorable environmental actions during their service life, leading to the mechanical properties degradation, moreover, cyclic loadings such as traffic loads, wind loads may further accelerate structural damage, therefore, improving durability of concrete is of vital for structures servicing in severe environment. Graphene oxide (GO), as a new nano-reinforced material, has ultra-high mechanical properties and large specific surface area as a concrete reinforcing material. This study entailed an examination of the properties of Graphene Oxide Concrete (GOC) with varying levels of GO incorporation (0, 0.02, 0.05, 0.08 wt%). It also encompassed an analysis of the fatigue properties of GOC under different stress levels and varying sulfate wetting and drying cycles. Additionally, the investigation delved into the degradation mechanisms affecting Graphene Oxide Concrete (GOC) when subjected to sulfate erosion conditions. Furthermore, the study assessed the mass loss of specimens and their fatigue life under diverse environmental conditions. The results showed that appropriate GO incorporations could enhance concrete's mechanical and fatigue properties after sulfate attack. In addition, scanning electron microscope (SEM) analysis showed that GO could adjust the aggregation state of cement hydration products and its own reaction with some cement hydration crystals to form strong covalent bonds, to improve and enhance microstructural denseness.

KEYWORDS

graphene oxide, mechanical property, sulfate corrosion, fatigue life, concrete, SEM

1 Introduction

In recent years, with the rapid development of nanomaterials, scholars have been researching ways to improve structural performance (mechanical properties, durability, and long-term performance, etc.) by incorporating nanomaterials (Zhang and Li, 2011; Ali et al., 2013; Zhu et al., 2022; Gul et al., 2023). However, the application of nanotechnology in construction engineering is complex (Pacheco-Torgal and Jalali, 2011). The main nanomaterials currently incorporated into concrete are carbonaceous nanomaterials, nano metals and metal oxides and inorganic nanomaterials. Among them, GO is one of hot spots in nanomaterial researches (Chen et al., 2018; Li et al., 2018; Lu et al., 2018). The oxygen-containing functional groups make the GO-dispersion hydrophilic and dispersive (Dreyer et al., 2014), which can help forming hydration products. These make hydration products interweave and penetrate into a uniform and dense microstructure (Raki et al.,

2010; Amin and Abu el-Hassan, 2015; Nirmala and Dhanalakshmi, 2015), resulting in microcosmic defect reductions (Zhao et al., 2020), and thus significantly improve the strength, toughness, and durability of cement composites (Peng et al., 2019).

Lv et al. (2013) investigated the effect of GO nanosheets on the microstructure and mechanical properties of cement composites. They showed that GO nanosheets could modulate the formation of flower-like crystals and significantly enhance the tensile and flexural strength of the materials. Jiang et al. (2018) studied the effects of GO and polyvinyl alcohol (PVA) fibers on the mechanical properties, durability, and microstructure of cement materials, and the results showed that the addition of polyvinyl alcohol fibers and GO significantly enhanced the mechanical strength and durability of cement-based materials. Gong et al. (2015) also demonstrated that the usage of GO in cement composites and mortar could enhance their mechanical properties.

On the other hand, sulfate attack is one of main reasons that may reduce durability of concrete (Zhang et al., 2021), developing high-performance concrete has critical engineering applications (Han and Tian, 2018). Yang et al. (2017) used long-term immersion to simulate structures immersed in seawater or groundwater to study the corrosion resistance, and the test results showed that incorporating GO could significantly improve the corrosion resistance coefficient of concrete. Cheng et al. (2021) investigated the durability performance of concrete specimens exposed to sulfate attack, the results showed that the integral area of sulfate ion distribution was a suitable index to describe the nonhomogeneous deterioration behavior of sulfate-attacked concrete. Mohammed et al. investigated the effect of GO on concrete properties by experiment, which showed that GO enhanced resistance to chloride attack and water permeability (Mohammed et al., 2015), demonstrating that GO could refine the pore structure of cementitious materials (Mohammed et al., 2016).

For GOC, a new high-performance concrete material, there are few studies on its durability and fatigue performance under sulfate attack. Since the applications of GO nanomaterials in constructions will significantly impact properties and durability of structures in long term, it is necessary to investigate the degradation mechanism of GOC under corrosive environments, to comprehensively understand the performance of this new material and its application in concrete structures. This study concerns GO nanomaterials' effects on mechanical properties of concrete, and mainly focus on the degradation of mechanical properties of GOC in sulfate erosion environments as well as its fatigue performance after sulfate attack, by conducting static loading test and fatigue loading test. In which, different stress levels and number of cycles are taken into account, to understand if these variable factors will impact on the fatigue performance of GO concrete.

2 Experimental investigation

2.1 GOC material

The specimens were prepared in accordance with Chinese code GB/T 50081 (Ministry of Housing and Urban-Rural Construction of China, 2019), having standard dimensions of 100 mm × 100 mm × 100 mm and consisting of complex Portland cement, multilayer GO-dispersion, aggregates (crushed stone as coarse aggregates and manufactured sand as fine aggregates) and water.

TABLE 1 The components of the P.C. 42.5.

Components of P.C. 42.5	Percentage (%)
CaO	65.32
SiO_2	21.48
Al_2O_3	4.12
Fe_2O_3	3.22
MgO	2.82
K_2O	0.93
SO_3	0.68
Na_2O	0.47
TiO_2	0.19
P_2O_5	0.10
MnO	0.06
Loss on ignition	0.56

TABLE 2 The physical parameters and chemical components of GO.

	Specification	Contents
Physical parameters	Purity	>95 wt%
	Thickness	3.42–7.82 nm
	Layers	0.79 nm
	Specific surface area	130–260 m^2/g
	Lamellar diameter	12–40 μm
Chemical components (from XRD test)	C	69.26 %
	O	30.16 %
	S	0.28 %
	Si	0.16 %
	Cl	0.11 %

2.1.1 Complex portland cement

All indexes (fineness, stability, mechanical properties, etc.) of P.C. 42.5 complex Portland cement meet the requirements of Chinese code GB175 (Chinese Standards Institute, 2020). 3 and 28 days flexural strengths are no less than 3.5 and 6.5 MPa, respectively, while compressive strengths are no less than 15 and 42.5 MPa, respectively. Its chemical composition is shown in Table 1.

2.1.2 Multilayer GO-dispersion

The multilayer GO was frozen, dried and dispersed by the modified *Hummers* method (Hummers and Offeman, 1958), and the finished product had no precipitation but good dispersion. Its dispersion is black oily liquid with a concentration of 10 mg/mL. The parameters and components of GO are shown in Table 2.

TABLE 3 The particle gradation of fine aggregates.

Nominal diameter (mm)	0	0.15	0.3	0.6	1.18	2.38	4.72
Accumulated sieve residue (%)	100	89.34	74.98	52.96	37.45	18.76	0.96

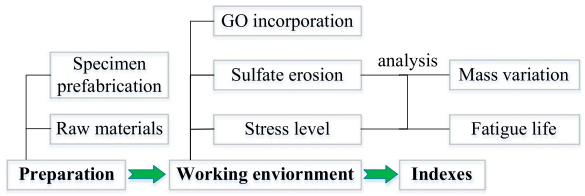

FIGURE 1
Test Procedure.

2.1.3 Concrete aggregates

The coarse aggregate of GOC specimens is 5–20 mm grade crushed stone, and the fine aggregate is manufactured sand, whose details are shown in Table 3.

2.2 Specimen testing

The test procedure in this study is shown in Figure 1.

2.2.1 Preparation for specimens

The tested GOC specimens were all with a water-cement ratio of 0.50 and a sand rate of 35%, and the GO-dispersions of 0, 0.02, 0.05, 0.08wt% (the mass ratio of GO to cement) were thoroughly mixed with water before the test. The concrete was configured according to the mixture proportion (Table 4) and injected into the cube mold of 100 mm × 100 mm × 100 mm, finally, the marked specimens were put into the curing room and cured in standard conditions. All the above procedures were completed according to the requirements of Chinese code GB/T50082 (Ministry of Housing and Urban-Rural Construction of China, 2009).

2.2.2 Test situation

1) Load test after sulfate attack

Na_2SO_4 solution with a mass fraction of 10 wt% was added into the test chamber, and specimens were subjected to 0, 30, 60, 90, and 120 dry-wet cycles according to the cyclic system. The fabricated samples were named according to the test environment and GO incorporation; for example, SA_{30}-$GOC_{0.02\%}$ indicated sulfate erosion GOC with 30 wetting and drying cycles and 0.02 wt% GO.

2) Fatigue test after sulfate attack

Another 18 prisms GO concrete specimens (marked as S45-FGOC-*a*-1~3 and S90-FGOC-*a*-1~3, respectively) were fabricated for fatigue testing, where S45 and S90 represented the specimens underwent 45 times and 90 times sulfate wetting and drying cycles, respectively; *a* represented the stress level, which was individually set as 0.75, 0.80 and 0.85 in the fatigue test. To be comparable, the counterpart specimens without sulfate erosion were also accordingly prepared to carry out the same fatigue test. The axial compression fatigue test was carried out by an electrohydraulic servo fatigue testing machine. The test parameters were set according to the load test results. Fatigue loading was carried out in a load-controlled manner, and the fatigue loading was carried out in the form of a sin-constant amplitude load spectrum. The cyclic loading started, ranging from the minimum fatigue stress to the maximum fatigue stress at the specific frequency of 10 Hz. Herein, the stress ratio was the ratio of the minimum fatigue stress to the maximum fatigue stress and was set at 0.1 in this study.

3) Measurement indexes

This test was referenced to Chinese code GB/T 50081 (Ministry of Housing and Urban-Rural Construction of China, 2019), and the measurements included mass and fatigue life. The detailed steps were as follows:

a. When the cycle number reached to the test design values, specimens were firstly dried to observe surface damages.
b. Then the mass of each specimen was measured and recorded in detail.
c. The prism specimens were taken fatigue load, the stress level and fatigue life were measured during the test.
d. Fractures of the specimens were observed using the Quattro setup, to investigate the effect of GO incorporation on concrete microstructure at different cycle counts.

TABLE 4 Test design and mixture proportion (unit: kg/m³).

Specimen No.	Cement	Manufactured sand	Crushed stone		Water	GO
			5–10 mm	10–20 mm		
$GOC_{0\%}$	398	623	450	734	195	0
$GOC_{0.02\%}$	398	623	450	734	195	0.080
$GOC_{0.05\%}$	398	623	450	734	195	0.199
$GOC_{0.08\%}$	398	623	450	734	195	0.318

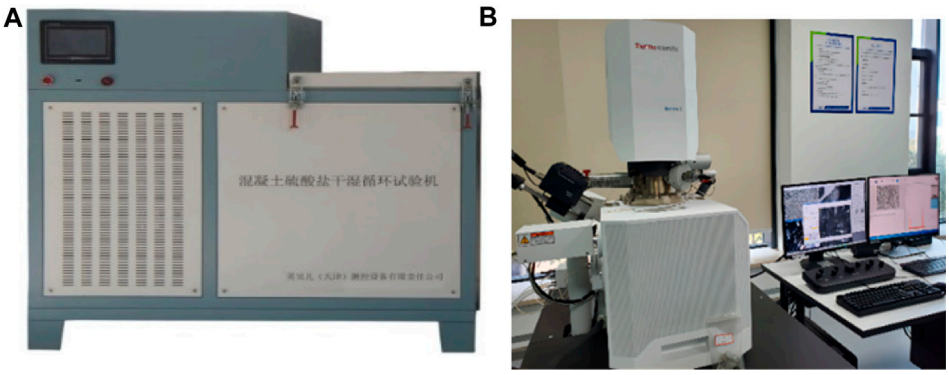

FIGURE 2
Test setup **(A)** IMGS-54 setup for sulfate attack; **(B)** Quattro setup for SEM.

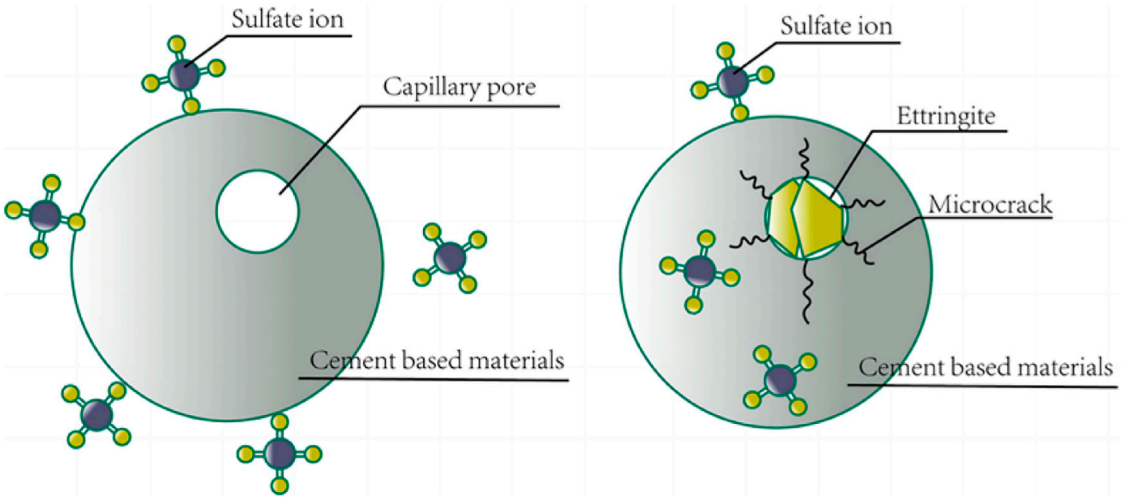

FIGURE 3
Schematic diagram of damage to concrete under sulfate attack.

The environmental and mechanical test setup described in this section was shown in Figure 2.

3 Results and discussion

In this study, properties of GOC with different GO incorporations (0, 0.02, 0.05, 0.08 wt%, respectively) and fatigue properties of GOC with different stress level and sulfate wetting and drying cycles were tested. Generally speaking, GO incorporation was in the range of 0–0.08 wt%, GO can disperse nicely, participate in and regulate the cement hydration process, making the formation and aggregation of cement hydration products more regular and effective, reducing the cracks and pores inside the concrete. There were physical and chemical reactions. Graphene oxide had excellent mechanical strength and stiffness, and its plate structure could prevent sulfate from invading the interior of concrete, thereby improving the ability to resist sulfate corrosion. At the same time, the high surface area and functional groups of GO may also adsorb and hydrate with sulfate ions, thereby forming protection inside the concrete.

3.1 Appearance phenomena

The sulfate attack of concrete can be divided into two main categories: physical and chemical erosion (Liu et al., 2011). During the physical attack, the cracking damage of concrete is caused by the swelling stress generated around the concrete's pore walls, which is greater than the tensile strength of concrete, and the swelling stress originates from the pressure generated by the crystals on the pore walls. During the chemical attack, sulfate ions react with cement hydration products to produce swelling products, which are about 2.5 times larger than the initial reaction phase, thus causing swelling cracking of concrete (Neville, 1995; Leng et al., 2012), as shown in Figure 3.

This damage usually causes peeling, and many micro-cracks appear on the surface of concrete specimens. The specimens show spalling at the edges and corners when the attack is aggravated. As shown in Figure 4, the GO-doped specimens maintained good integrity, and the surface condition remained intact in the less severe case (60 cycles). In the case of severe erosion (120 cycles), both GO-doped and non-GO-doped specimens were severely

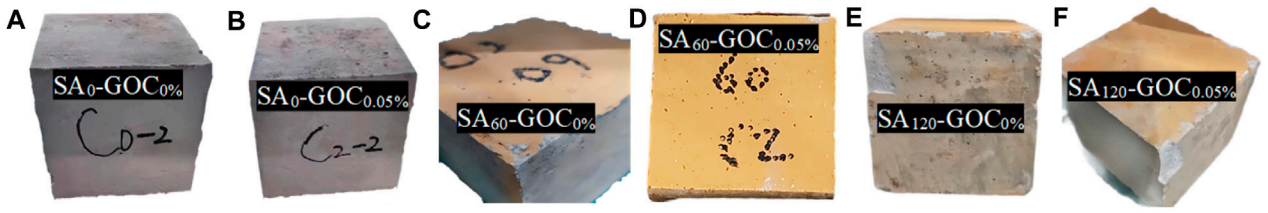

FIGURE 4
The appearance of specimens under the sulfate attack test.

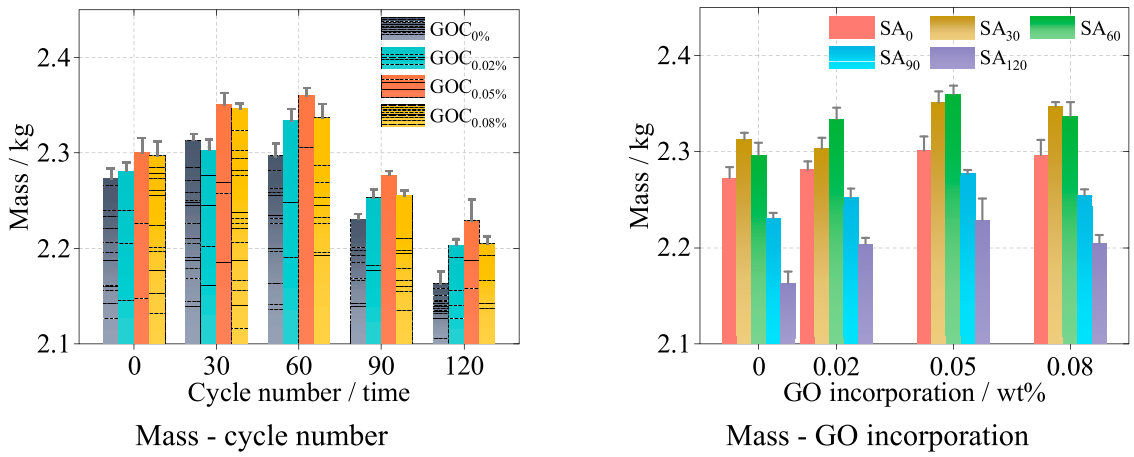

FIGURE 5
The mass of specimens under the sulfate attack test.

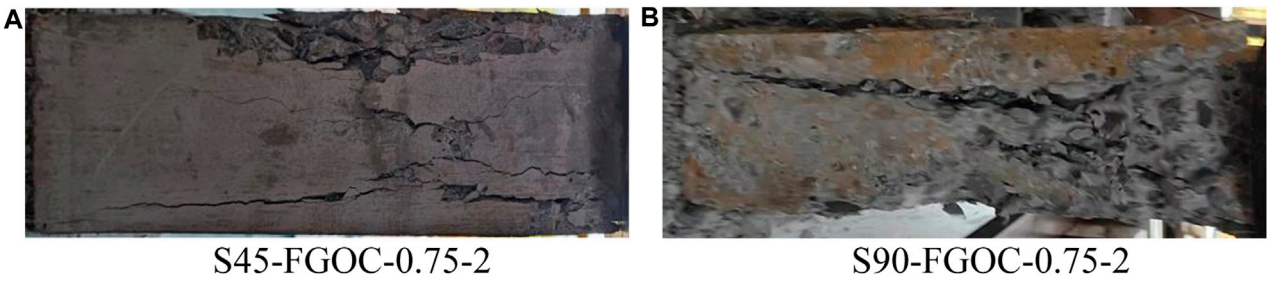

FIGURE 6
Failure mode of sulfate erosive specimens under fatigue testing.

damaged, compared to the GO-doped specimens, which had relatively good integrity and fewer internal traces of sulfate attack.

3.2 Mass variation

Figure 5 shows the mass variation of the specimens under the sulfate attack test. The results show that the masses of all specimens showed a trend of "first increase and then decrease" with the increase of cycle time and GO incorporation, respectively, and the masses of GOC specimens with 60 cycles and 0.05 wt% GO increased most significantly. The mass of all specimens was higher than the initial mass for 30–60 cycles and lower than the initial mass for 90–120 cycles. After the specimens started to show a mass loss, the mass loss rate of GO-doped specimens was significantly lower than that of the non-GO-doped specimens. For example, the mass loss rate of GO-doped specimens ranged from 3.073% to 3.991% after 120 cycles, compared with 4.839% for non-GO-doped specimens. The test results indicate that GO enhances the performance of concrete in resisting mass loss under the action of a sulfate attack environment.

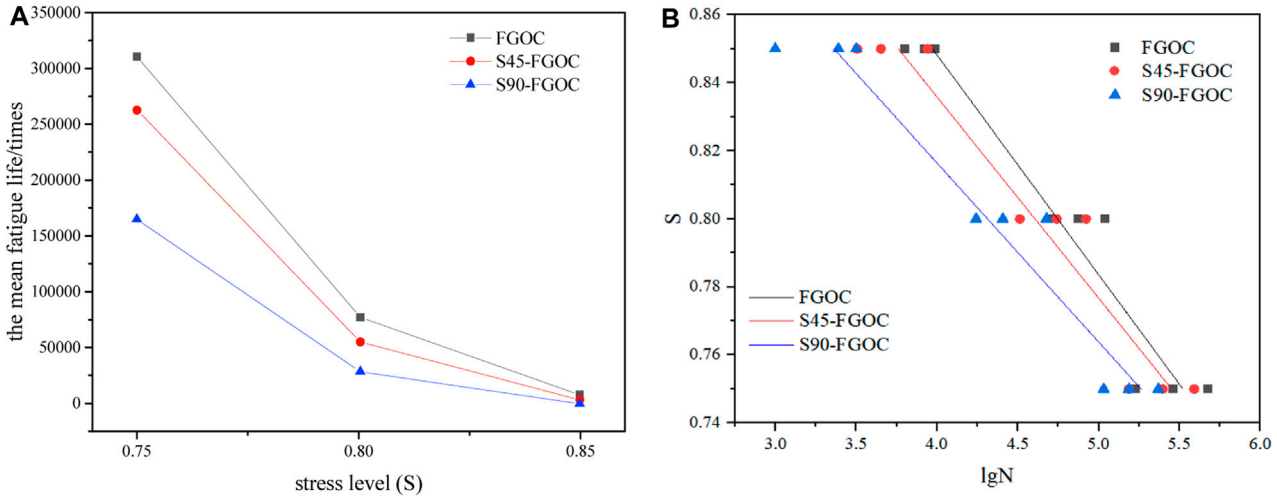

FIGURE 7
Relationship between fatigue life and stress level: **(A)** Mean fatigue life vs stress level, and **(B)** S-N curves.

TABLE 5 Linear regression results for general environmental condition.

Specimen number	Fatigue life *Ni*	ln*Ni*	Survival Rate *P*	ln[ln(1/*P*)]	*b*	*a*
FOC-0.75-1	135537	11.817	0.75	−1.2459	1.568	−19.747
FOC-0.75-2	226534	12.331	0.50	−0.3665		
FOC-0.75-3	369827	12.821	0.25	0.3266		
FOC-0.80-1	36558	10.507	0.75	−1.2459	1.677	−18.777
FOC-0.80-2	53344	10.885	0.50	−0.3665		
FOC-0.80-3	91831	11.428	0.25	0.3266		
FOC-0.85-1	2496	7.822	0.75	−1.2459	1.361	−11.941
FOC-0.85-2	5652	8.640	0.50	−0.3665		
FOC-0.85-3	7383	8.907	0.25	0.3266		
FGOC-0.75-1	168641	12.036	0.75	−1.2459	1.519	−19.506
FGOC-0.75-2	288475	12.572	0.50	−0.3665		
FGOC-0.75-3	475368	13.072	0.25	0.3266		
FGOC-0.80-1	51917	10.857	0.75	−1.2459	1.717	−19.609
FGOC-0.80-2	74583	11.220	0.50	−0.3665		
FGOC-0.80-3	109532	11.604	0.25	0.3266		
FGOC-0.85-1	6338	8.7543	0.75	−1.2459	1.897	−17.172
FGOC-0.85-2	8449	9.042	0.50	−0.3665		
FGOC-0.85-3	9746	9.185	0.25	0.3266		

3.3 Fatigue properties

The maximum fatigue load was determined by the mean value of ultimate load for the static load test, multiplying the stress level, while the minimum fatigue load was then calculated by the stress ratio of 0.1. The failure mode of specimens was shown in Figure 6.

As seen, specimens seriously damaged with wide cracks and local concrete collapse. A large amount of concrete debris fell off in Figure 6B, indicating specimens under 90 times sulfate wetting and drying cycles suffering severer damages. The relationship between fatigue life of specimens and stress level was plotted in Figure 7. In which, (a) compared the mean fatigue life of normal GO concrete

TABLE 6 Linear regression results for sulfate erosion condition.

Specimen number	Fatigue life *Ni*	ln*Ni*	Survival Rate *P*	ln[ln(1/*P*)]	*b*	*a*
S45-FGOC-0.75-1	153523	11.942	0.75	−1.2459	1.691	−21.415
S45-FGOC-0.75-2	248765	12.424	0.50	−0.3665		
S45-FGOC-0.75-3	389501	12.873	0.25	0.3266		
S45-FGOC-0.80-1	32488	10.389	0.75	−1.2459	1.666	−18.553
S45-FGOC-0.80-2	54981	10.915	0.50	−0.3665		
S45-FGOC-0.80-3	83541	11.333	0.25	0.3266		
S45-FGOC-0.85-1	3204	8.072	0.75	−1.2459	1.494	−13.154
S45-FGOC-0.85-2	4497	8.411	0.50	−0.3665		
S45-FGOC-0.85-3	8742	9.076	0.25	0.3266		
S90-FGOC-0.75-1	107455	11.585	0.75	−1.2459	2.014	−24.531
S90-FGOC-0.75-2	154331	11.947	0.50	−0.3665		
S90-FGOC-0.75-3	233764	12.362	0.25	0.3266		
S90-FGOC-0.80-1	17407	9.765	0.75	−1.2459	1.521	−15.984
S90-FGOC-0.80-2	25518	10.147	0.50	−0.3665		
S90-FGOC-0.80-3	47554	10.770	0.25	0.3266		
S90-FGOC-0.85-1	998	6.906	0.75	−1.2459	1.262	−10.006
S90-FGOC-0.85-2	2451	7.804	0.50	−0.3665		
S90-FGOC-0.85-3	3166	8.060	0.25	0.3266		

TABLE 7 Linear regression results for freeze-thaw condition.

Specimen number	Fatigue life *Ni*	ln*Ni*	Survival Rate *P*	ln[ln(1/*P*)]	*b*	*a*
D75-FGOC-0.75-1	130547	11.779	0.75	−1.2459	1.683	−21.110
D75-FGOC-0.75-2	243433	12.403	0.50	−0.3665		
D75-FGOC-0.75-3	322520	12.684	0.25	0.3266		
D75-FGOC-0.80-1	31464	10.357	0.75	−1.2459	1.944	−21.427
D75-FGOC-0.80-2	54522	10.906	0.50	−0.3665		
D75-FGOC-0.80-3	68534	11.135	0.25	0.3266		
D75-FGOC-0.85-1	3185	8.066	0.75	−1.2459	1.750	−15.230
D75-FGOC-0.85-2	4327	8.373	0.50	−0.3665		
D75-FGOC-0.85-3	7552	8.930	0.25	0.3266		
D150-FGOC-0.75-1	76553	11.246	0.75	−1.2459	1.837	−21.762
D150-FGOC-0.75-2	101568	11.528	0.50	−0.3665		
D150-FGOC-0.75-3	173764	12.065	0.25	0.3266		
D150-FGOC-0.80-1	13407	9.504	0.75	−1.2459	2.018	−20.467
D150-FGOC-0.80-2	22518	10.022	0.50	−0.3665		
D150-FGOC-0.80-3	28554	10.260	0.25	0.3266		
D150-FGOC-0.85-1	868	6.766	0.75	−1.2459	1.915	−14.011
D150-FGOC-0.85-2	1351	7.209	0.50	−0.3665		
D150-FGOC-0.85-3	1684	7.429	0.25	0.3266		

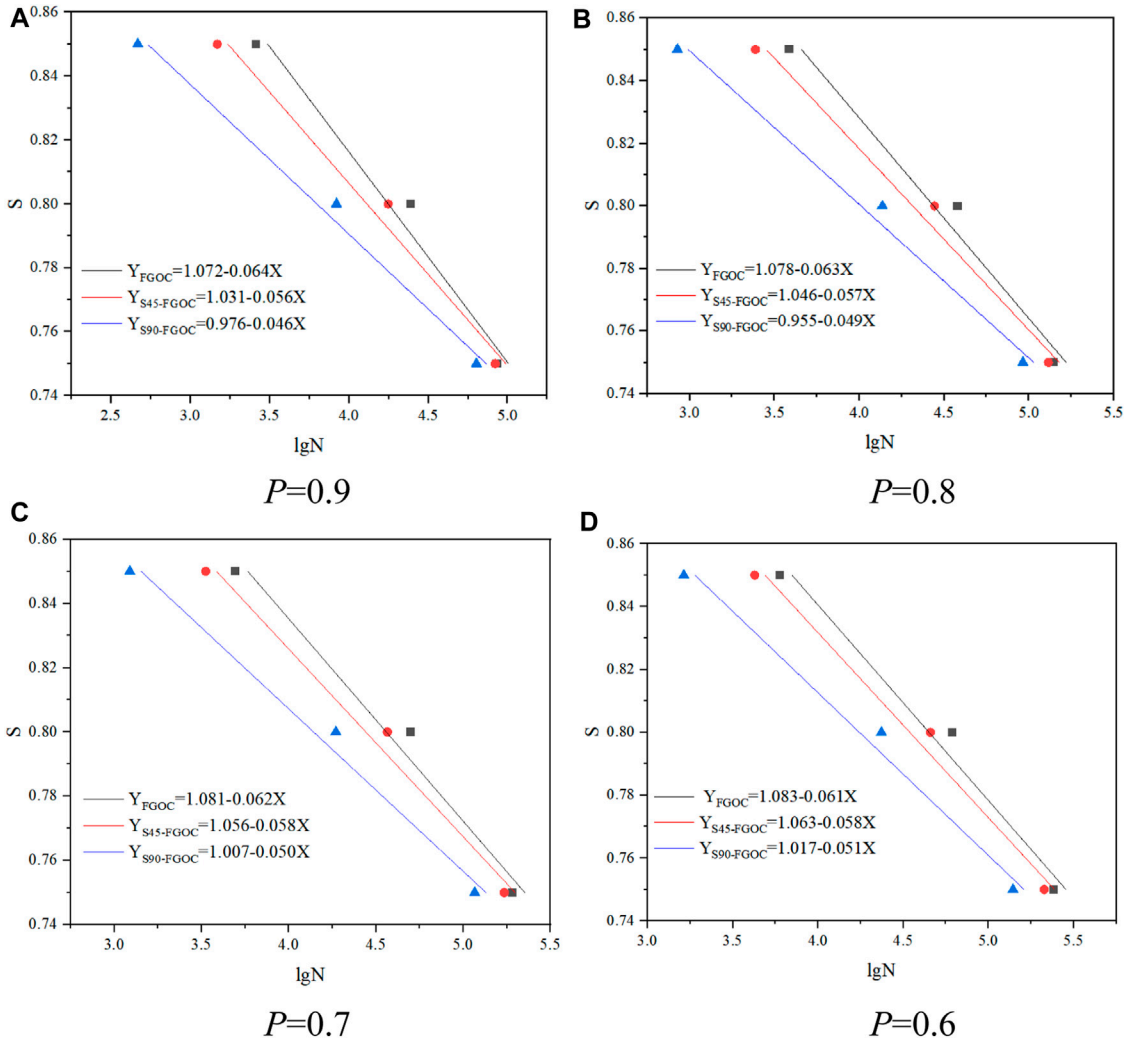

FIGURE 8
Linear regression equations for sulfate condition.

with that of GO concrete with sulfate erosion, and (b) showed the corresponding *S-N* curves. It can be seen in both two figures, high stress level and sulfate erosion would remarkably reduce fatigue life.

3.3.1 Weibull distribution

The Weibull distribution is a widely used probability distribution that is used to depict the correlation between an object's life and various factors such as stress, strain, or durability (Zhang et al., 2019; Zhang et al., 2020a; Zhang et al., 2020b; Zhang et al., 2022). Previous studies show that a Weibull distribution is proper for fatigue estimation of concrete materials (Hong et al., 2020). Therefore, a Weibull distribution is used to assess fatigue life of concrete specimens in this study, which can be expressed as

$$\boldsymbol{ln[ln(1/P)] = blnN_P - blnN_a} \quad (1)$$

in which, P is the survival rate; N_p is the fatigue life, N_a is the characteristic life parameter; and b is the slope of the linear equation.

The empirical formula of survival rate P is

$$\boldsymbol{P = 1 - \frac{i}{1+k}} \quad (2)$$

where i is the serial number of the test specimen according to the fatigue life from low to high; and n is the number of test specimen per group.

Letting the Weibull parameters $Y = ln[ln(1/P)]$, $X = lnN_P$ and, $a = -blnN_a$, then using $Y = bX+a$ to conduct Weibull distribution tests on the fatigue life of specimens at different stress levels. The results by linear regression analysis for general environmental condition, sulfate erosion condition and freeze-thaw condition were listed in Tables 5–7 as below.

3.3.2 Fatigue equation and S-N curve

Fatigue equation is usually used to present the relationship between fatigue life N and stress level S, by which, the stress level and cycle number can be obtained when structure fails. The fatigue equation can also be expressed by curves in logarithmic coordinates, namely, the so-

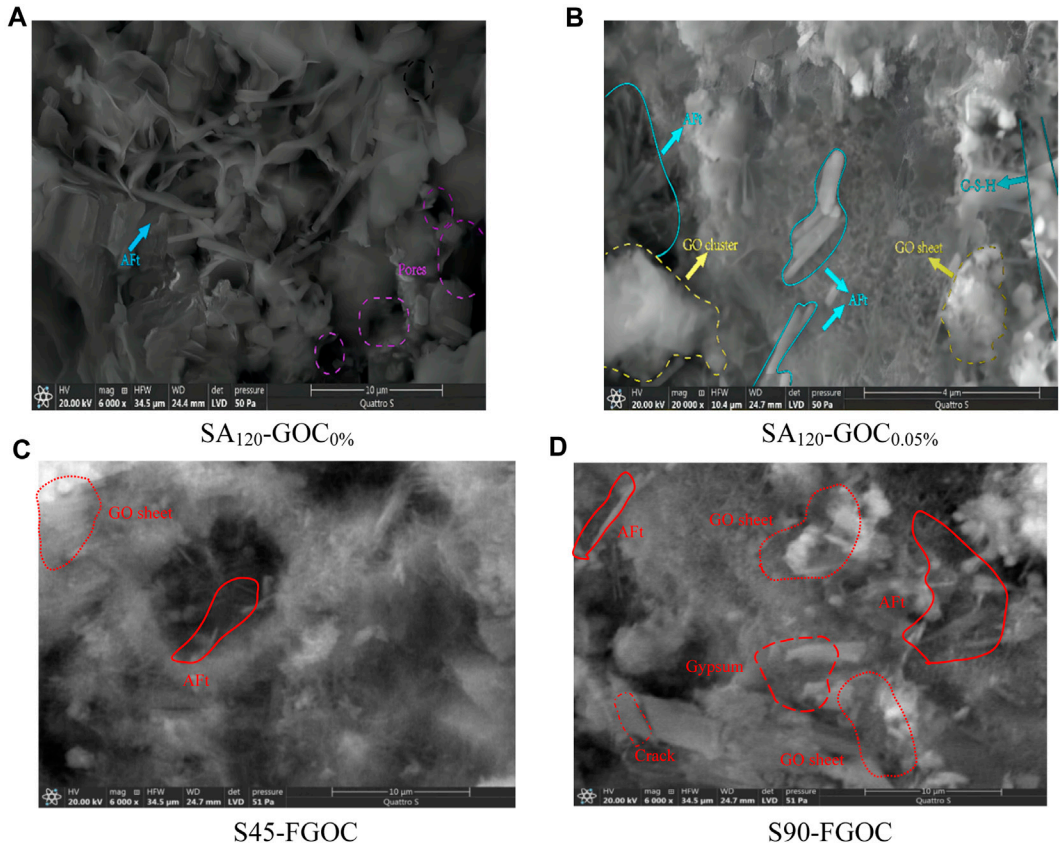

FIGURE 9
The SEM images of specimens under the sulfate attack test.

called *S-N* curve, to demonstrate fatigue characteristics of materials. The fatigue equation can be expressed as

$$S = AlgN + B \tag{3}$$

in which, S donates the stress level; N is the fatigue life; A and B are coefficients.

Note that a survival rate of 0.5 is taken in default and failure probability is not covered in Equation 3, for structure safety, fatigue equation with higher survival rate needs to establish. Taking the regression results of Weibull distribution, the fatigue life with survival rate P could be calculated by Equation 4, where the parameters are the same as before. Let N_p replace N, then fatigue life considering different survival rates could be obtained. In this study, four survival rates of 0.6, 0.7, 0.8 and 0.9 were taken.

$$N_P = exp\frac{ln(ln(1/P)) - a}{b} \tag{4}$$

Figure 8 depicts the linear regression equation that represents the relationship between sulfate corrosion and various survival rates. The observation depicted in Figure 8A reveals a steady decrease in the fatigue properties of GOC specimens as the number of sulfate dry and wet cycles increases, while maintaining a constant stress level, when the survival rate P is 0.9. The sensitivity of the sample to stress increases in proportion to the extent to which it is influenced by the frequency of sulfate exposure during dry and wet cycles. Furthermore, it is evident from Figures 8A–D that as the survival rate P lowers from 0.9 to 0.6, there is a rise in the horizontal coordinate values for each set of curves. The findings indicate that the fatigue life of GOC specimens exhibits an upward trend when the survival rate P decreases following various durations of sulfate dry and wet cycling.

3.4 SEM

To explain the results obtained in the previous section, the microstructure of specimens with different GO incorporations under 120 sulfate dry-wet cycles was compared and analyzed. The SEM images are shown in Figure 9. Figure 9A shows a large number of AFt produced by sulfate attack in non-GO-doped specimens. These AFt crystals are arranged disorderly, and there are many cracks and pores around them, further aggravating the attack of sulfate ions on concrete. When some amount of GO is incorporated, GO sheets and clusters appear in large-scale agglomeration or clustering (Figure 9B). Many cement hydration crystals are distributed around them in a disorganized manner, the number of pores increases, the denseness of microstructure decreases, and the load transfer efficiency between cement matrix and GO is affected and starts to decrease, which instead affects the concrete resistance to sulfate attack. As seen in Figures 9C, D, GO

sheets prevented interior concrete from sulfate eroding at some extent, but with the occurrence of cracks on GO sheets, the structural fatigue performance declined and finally failed.

The results show that, on the one hand, GO can reduce the number of products produced by sulfate attack so that the microstructure of concrete remains relatively dense when subjected to sulfate attack. On the other hand, it improves the erosion resistance of concrete by promoting the generation of regular cement hydration products and optimizing the crystal arrangement to reduce the size and number of micro-cracks and pores.

4 Conclusion

This paper tested the mechanical and fatigue properties of GOC under sulfate erosion. The test results were given and explained concerning the mechanical behavior of GO cement paste and the microstructures of GO cement paste observed by SEM. The following conclusions can be obtained in this study:

1) For the sulfate erosion environment, the degradation of the mechanical properties of concrete-resistant sulfate attack was significantly improved by incorporating GO, and this enhancement was most significant at 0.05 wt% GO incorporation.
2) Sulfate erosion would accelerate fatigue damage accumulation in concrete, then remarkably reduce fatigue life and strength. But comparatively, stress level would affect the fatigue life more seriously. While Weibull distribution can be used to assess the fatigue life of GO concrete under any environmental conditions.
3) It can be seen from SEM microstructure that GO sheets generally improved the compactness of concrete and restrained crack development and spread further, even under severe environmental condition, GO sheets could also relieve sulfate erosion damage.

Data availability statement

The raw data supporting the conclusion of this article will be made available by the authors, without undue reservation.

Author contributions

XW: Conceptualization, Methodology, Resources, Writing–original draft. GZ: Data curation, Formal Analysis, Software, Writing–original draft. LL: Methodology, Writing–original draft, Writing–review and editing. YL: Validation, Visualization, Writing–original draft. HK: Data curation, Writing–original draft. CZ: Software, Writing–original draft.

Funding

The authors declare financial support was received for the research, authorship, and/or publication of this article. This research was funded by the Natural Science Foundation of Chongqing (Grant No. CSTB2022NSCQ-MSX1655) and the State Key Laboratory of Structural Dynamics of Bridge Engineering and Key Laboratory of Bridge Structure Seismic Technology for Transportation Industry Open Fund (Grant No. 202205).

Conflict of interest

Author CZ was employed by Shenzhen Y. S. Mao Bridge Design Group Co Ltd.

The remaining authors declare that the research was conducted in the absence of any commercial or financial relationships that could be construed as a potential conflict of interest.

Publisher's note

References

Ali, M., Li, X., and Chouw, N. (2013). Experimental investigations on bond strength between coconut fibre and concrete. *Mater. Des.* 44, 596–605. doi:10.1016/j.matdes.2012.08.038

Amin, M., and Abu el-Hassan, K. (2015). Effect of using different types of nano materials on mechanical properties of high strength concrete. *Constr. Build. Mater* 80, 116–124. doi:10.1016/j.conbuildmat.2014.12.075

Chen, Z., Zhou, X., Wang, X., and Guo, P. (2018). Mechanical behavior of multilayer GO carbon-fiber cement composites. *Constr. Build. Mater* 159, 205–212. doi:10.1016/j.conbuildmat.2017.10.094

Cheng, H., Liu, T., Zou, D., and Zhou, A. (2021). Compressive strength assessment of sulfate-attacked concrete by using sulfate ions distributions. *Constr. Build. Mater* 293, 123550. doi:10.1016/j.conbuildmat.2021.123550

Chinese Standards Institute (2020). *Common Portland cement (GB175-2020)*. Beijing, China: Chinese Standards Institute.

Dreyer, D. R., Todd, A. D., and Bielawski, C. W. (2014). Harnessing the chemistry of graphene oxide. *Chem. Soc. Rev.* 43, 5288–5301. doi:10.1039/C4CS00060A

Gong, K., Pan, Z., Korayem, A. H., Qiu, L., Li, D., Collins, F., et al. (2015). Reinforcing effects of graphene oxide on Portland cement paste. *J. Mater Civ. Eng.* 27, A4014010. doi:10.1061/(ASCE)MT.1943-5533.0001125

Gul, W., Akbar Shah, S. R., Khan, A., Ahmad, N., Ahmed, S., Ain, N., et al. (2023). Synthesis of graphene oxide (GO) and reduced graphene oxide (rGO) and their application as nano-fillers to improve the physical and mechanical properties of medium density fiberboard. *Front. Mater* 10, 1206918. doi:10.3389/fmats.2023.1206918

Han, N., and Tian, W. (2018). Experimental study on the dynamic mechanical properties of concrete under freeze–thaw cycles. *Struct. Concr.* 19, 1353–1362. doi:10.1002/suco.201700170

Hong, F., Oiao, H., and Wang, P. (2020). Predicting the life of BNC-coated reinforced concrete using the Weibull distribution. *Emerg. Mater Res.* 9, 1–10. doi:10.1680/jemmr.19.00087

Hummers, W. S., and Offeman, R. E. (1958). Preparation of graphitic oxide. *J. Am. Chem. Soc.* 80, 1339. doi:10.1021/ja01539a017

Jiang, W., Li, X., Lv, Y., Zhou, M., Liu, Z., Ren, Z., et al. (2018). Cement-based materials containing graphene oxide and polyvinyl alcohol fiber: mechanical properties, durability, and microstructure. *Nanomaterials* 8, 638. doi:10.3390/nano8090638

Leng, F. G., Zhou, Y. X., and Wang, J. (2012). *Inspection and assessment of concrete durability*. Beijing, China: China Building Materials Press.

Li, G., Yuan, J. B., Zhang, Y. H., Zhang, N., and Liew, K. M. (2018). Microstructure and mechanical performance of graphene reinforced cementitious composites. *Compos Part A-Appl S* 114, 188–195. doi:10.1016/j.compositesa.2018.08.026

Liu, Z., Deng, D., De Schutter, G., and Yu, Z. (2011). Micro-analysis of "salt weathering" on cement paste. *Cem. Concr. Comp.* 33, 179–191. doi:10.1016/j.cemconcomp.2010.10.010

Lu, L., Zhao, P., and Lu, Z. (2018). A short discussion on how to effectively use graphene oxide to reinforce cementitious composites. *Constr. Build. Mater* 189, 33–41. doi:10.1016/j.conbuildmat.2018.08.170

Lv, S., Ma, Y., Qiu, C., Sun, T., Liu, J., and Zhou, Q. (2013). Effect of graphene oxide nanosheets of microstructure and mechanical properties of cement composites. *Constr. Build. Mater* 49, 121–127. doi:10.1016/j.conbuildmat.2013.08.022

Ministry of Housing and Urban-Rural Construction of China (2009). *Standard for test methods of long-term performance and durability of ordinary concrete (GB/T 50082-2009)*. Beijing, China: China Architecture & Building Press.

Ministry of Housing and Urban-Rural Construction of China (2019). *Standard for test methods of concrete physical and mechanical properties (GB/T50081-2019)*. Beijing, China: China Architecture & Building Press.

Mohammed, A., Sanjayan, J. G., Duan, W. H., and Nazari, A. (2015). Incorporating graphene oxide in cement composites: a study of transport properties. *Constr. Build. Mater* 84, 341–347. doi:10.1016/j.conbuildmat.2015.01.083

Mohammed, A., Sanjayan, J. G., Duan, W. H., and Nazari, A. (2016). Graphene oxide impact on hardened cement expressed in enhanced freeze–thaw resistance. *J. Mater Civ. Eng.* 28, 04016072. doi:10.1061/(ASCE)MT.1943-5533.0001586

Neville, A. M. (1995). *Properties of concrete*. Longman London: National Academies.

Nirmala, J., and Dhanalakshmi, G. (2015). Influence of nano materials in the distressed retaining structure for crack filling. *Constr. Build. Mater* 88, 225–231. doi:10.1016/j.conbuildmat.2015.04.022

Pacheco-Torgal, F., and Jalali, S. (2011). Nanotechnology: advantages and drawbacks in the field of construction and building materials. *Constr. Build. Mater s* 25, 582–590. doi:10.1016/j.conbuildmat.2010.07.009

Peng, H., Ge, Y., Cai, C. S., Zhang, Y., and Liu, Z. (2019). Mechanical properties and microstructure of graphene oxide cement-based composites. *Constr. Build. Mater* 194, 102–109. doi:10.1016/j.conbuildmat.2018.10.234

Raki, L., Beaudoin, J., Alizadeh, R., Makar, J., and Sato, T. (2010). Cement and concrete nanoscience and nanotechnology. *Materials* 3, 918–942. doi:10.3390/ma3020918

Yang, Y. L., Yuan, X. Y., Shen, X., and Yin, L. (2017). Research on the corrosion resistance of graphene oxide on cement mortar. *J. Funct. Mater* 48, 5144–5148. doi:10.3969/j.issn.1001-9731.2017.05.026

Zhang, C., Chen, W., Mu, S., Šavija, B., and Liu, Q. (2021). Numerical investigation of external sulfate attack and its effect on chloride binding and diffusion in concrete. *Constr. Build. Mater* 285, 122806. doi:10.1016/j.conbuildmat.2021.122806

Zhang, M., and Li, H. (2011). Pore structure and chloride permeability of concrete containing nano-particles for pavement. *Constr. Build. Mater* 25, 608–616. doi:10.1016/j.conbuildmat.2010.07.032

Zhang, Z. Y., Jin, X., Lin, S., and Bi, J. (2019). Direct shear behavior of sulfate-exposed shotcrete: experimental and modelling research. *Constr. Build. Mater* 210, 607–619. doi:10.1016/j.conbuildmat.2019.03.229

Zhang, Z. Y., Zhou, J. T., Yang, J., Zou, Y., and Wang, Z. (2020b). Cracking characteristics and pore development in concrete due to physical attack. *Mater Struct.* 53, 104–113. doi:10.1617/s11527-020-01541-5

Zhang, Z. Y., Zhou, J. T., Zou, Y., Yang, J., and Bi, J. (2020a). Change on shear strength of concrete fully immersed in sulfate solutions. *Constr. Build. Mater* 235, 117463. doi:10.1016/j.conbuildmat.2019.117463

Zhang, Z. Y., Zou, Y., Yang, J., and Zhou, J. T. (2022). Capillary rise height of sulfate in Portland-limestone cement concrete under physical attack: experimental and modelling investigation. *Cem. Concr. Comp.* 125, 104299. doi:10.1016/j.cemconcomp.2021.104299

Zhao, L., Guo, X., Song, L., Song, Y., Dai, G., and Liu, J. (2020). An intensive review on the role of graphene oxide in cement-based materials. *Constr. Build. Mater* 241, 117939. doi:10.1016/j.conbuildmat.2019.117939

Zhu, J., Jia, B., Di, Y., Liu, B., Wan, X., Wang, W., et al. (2022). Effects of graphene content on the microstructure and mechanical properties of alumina-based composites. *Front. Mater* 9, 965674. doi:10.3389/fmats.2022.965674